

Time course of changes in structure and morphology of chrysotile asbestos by dissolution

Hongo T.*

Work Environment Research Group, National Institute of Occupational Safety and Health, Japan, 6-21-1 Nagao, Tama-Ku, Kawasaki 214-8585, Japan

*corresponding author:

e-mail: peea.hongo@hotmail.co.jp

Present address: Department of Life Science and Green Chemistry, Faculty of Engineering, Saitama Institute of Technology, 1690 Fusaiji, Fukaya, Saitama 369-0293, Japan

Abstract The alteration of chrysotile by dissolution was investigated with the aim of revealing the effect of time course on its structure and morphology. At pH 1.3, both Mg and Si contained in chrysotile continued to dissolve for 28 days, and the extent of dissolution after 28 days of Mg was approximately four times greater than that of Si. As the dissolution time progressed, the octahedral sheets of magnesium hydroxide are destroyed and the residual silicon component transformed into amorphous silica. The dissolution reaction initially proceeds the outermost octahedral sheet of magnesium hydroxide. After 28 days, chrysotile altered into sheet-like form or fiber-like form formed by connecting nanoparticles, while there were fibers maintaining hollow structure.

Keywords: Chrysotile, Dissolution, Structure, Morphology, Fiber

1. Introduction

Chrysotile is the most widespread commercial form of asbestos, representing about 90% of the asbestos commercially employed in the last century (Mossman *et al.*, 1990). It is classified in the kaolin/serpentine mineral 1:1 group with trioctahedral site occupancy (Brindley and Brown, 1980). The chrysotile structure with the idealized chemical formula $Mg_3Si_2O_5(OH)_4$ is consisted of octahedral sheets of magnesium hydroxide covalently bonded to tetrahedral sheets of silicon oxide, with a regular layered structure. The lattice parameter of the octahedral layer is greater than that of the corresponding tetrahedral layer. The structural mismatch causes internal stress, which is released by the curvature of the layers. The curvature then leads to the fibrous and hollow-structured nature of chrysotile with the octahedral sheets located on the outer layer (Dana *et al.*, 1977). Naturally occurring bundles of chrysotile consist of regular sets of closely packed parallel nanofibers (Liu *et al.*, 2007).

In previous time, chrysotile was one of the most important inorganic materials for industrial applications and was widely used because of its excellent characteristics such as incombustible, thermally insulating and high electrical resistance. In addition, its fibers are strong and very

flexible (Foresti *et al.*, 2003). Afterward, as chrysotile was linked to a number of pulmonary health issues including asbestosis, mesothelioma and lung cancer, it is banned to use in many countries. At present, substitute materials have been developed and widely used.

The solubility of chrysotile has attracted attention among hygiene and engineering. Hygienists are interested in its biodurability in the lung, and engineers are interested in its conversion to non-hazardous phases and its application to CO₂ fixation technology (Hume & Rimstidt, 1992; Dlugogorski & Balucan, 2014). To evaluate accurately the

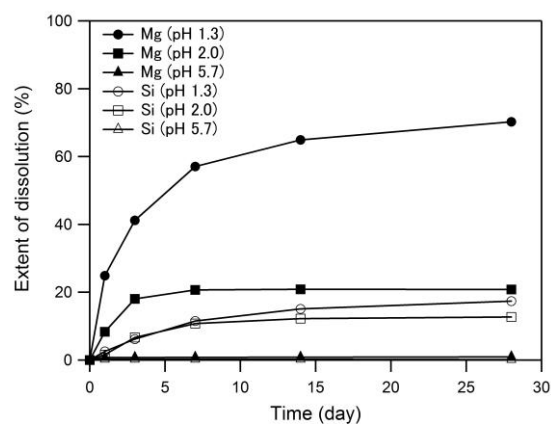


Figure 1. Extent of dissolution of Mg and Si from raw chrysotile as a function of time.

biodurability and its conversion to non-hazardous phases, it is very important to clearly understand the structural and morphological alterations that occur upon dissolution. The previous paper revealed the effect of pH on the dissolution rate of chrysotile and its structure (Hongo, 2016). However, it has not been thoroughly investigated the alteration of chrysotile by dissolution with time progressed. In this study, time course of change of chrysotile by dissolution was investigated. The effect of dissolution time on the structure of chrysotile and dissolution extent of magnesium and silicon from the chrysotile sample was investigated. Moreover, the morphology and structure of the dissolved residue were investigated by electron microscopy.

2. Experimental

2.1. Dissolution of chrysotile

All experiments were carried out on chrysotile collected from the Coalinga mine in New Idria (California, USA). The chemical composition was (mass%) SiO₂ 39.36, MgO 41.16, Fe₂O₃ 3.26, CaO 0.42, Al₂O₃ 0.41, Cr₂O₃ 0.30 with an ignition loss of 14.50 mass%, and a Mg/Si atomic ratio is 1.56.

Dissolution experiments were carried out in batch reactors at a solid/solution ratio of 2.0 mg/L. The chrysotile sample was placed directly in polypropylene bottles containing 100 mL of either a nitric acid solution at pH 1.3 or pH 2.0, or ion-exchanged water at pH 5.7. The reaction bottles were immersed in a shaking water bath kept at 37°C for 1–28 days. The residual solids were centrifuged at 3,000 rpm, washed with ion exchanged water 3 times, and dried at 80°C for 24 h. The supernatant was filtered through a 0.20 μm sieve.

2.2. Analysis and characterization

The initial pH of the nitric acid solutions and ion-exchanged water, and the filtrates after the dissolution experiments were measured at room temperature with an Orion Star A121 portable pH-meter (Thermo Scientific). The concentrations of dissolved magnesium and silicon in the filtrates were determined using inductivity coupled plasma optical emission spectrometry (ICP-OES, PerkinElmer, Optima 7300 DV). X-ray diffraction (XRD) patterns were obtained from the samples with a Rigaku RINT 2000 diffractometer using CuKα radiation. Room temperature Fourier transform infrared (FT-IR) spectra were recorded on a JASCO FT/IR 4100 spectrometer using KBr pellets. Field emission scanning electron microscopy (FE-SEM) images were obtained using a Hitachi S-4700 with an energy dispersive X-ray fluorescence spectrometer (EDX), by which the elemental mappings were performed. Transmission electron microscopy (TEM) observations were carried out on a JEOL JEM-2100 instrument operated at 200 kV.

3. Results and discussion

The extent of dissolution of Mg and Si from raw chrysotile as a function of time is shown in Fig. 1. The extent of dissolution was calculated on the assumption that the chemical composition of the raw chrysotile was ideal (i.e. Mg₃Si₂O₅(OH)₄), without impurities. The extent of dissolution of Mg was larger than that of Si, and as the pH was lower, the extent of dissolution increased for both Mg and Si. At initial pH 1.3, both Mg and Si continued to dissolve for 28 days, but the dissolution rate decreased with time. The extent of dissolution after 28 days of Mg was approximately four times greater (70.2%) than that of Si (17.4%). At initial pH 2.0, it hardly dissolved after 7 days. The extent of dissolution after 7 days was 20.7% for Mg and 10.8% for Si, but that after 28 days was 20.8 % for

Mg and 12.7% for Si. At initial pH 5.7, the dissolution rate was extremely slow, and the extent of dissolution after 28 days was 0.9 % for Mg and 0.2% for Si.

The pH values as a function of time is shown in Fig. 2. The pH increases after dissolution for all samples. The pH of the solution with the initial pH 1.3 gradually increased, and the pH became 1.9 after 28 days. Although slight pH increase was observed, the dissolution reaction continued to proceed for 28 days because the pH remained low (under pH 2). The pH of the solution with the initial pH 2.0 increased to 4.9 after 7 days, and the pH became 6.0 after 28 days. Previous study reported that the dissolution rate becomes extremely slow when the pH increased to approximately 5 (Hongo, 2016). Therefore, it is considered that the dissolution reaction hardly progressed after 7 days because of the pH increase. The pH of the solution with the initial pH 5.7 rapidly increased to pH 9.7 after 1 day and then remained almost constant at pH 10. The pH increase is due to the dissolution of the octahedral sheets of magnesium hydroxide, with an associated release of OH⁻ and Mg²⁺ ions (Hongo, 2016). A similar value was measured for a suspension of magnesium hydroxide (10.37) (Pundsack, 1955).

The XRD patterns obtained for raw chrysotile and for samples treated with nitric acid solution at pH 1.3 for 1–28 days are shown in Fig. 3. Two intense reflections are observed for raw chrysotile, at 2θ = 12.14° and 24.42°, which are indexed to the (002) and (004) planes (d = 7.29 and 3.64 Å, respectively) in agreement with ICDD file No. 25-0645. Low-concentration brucite and calcite impurities were evidenced at 2θ = 18.66° and 2θ = 29.44°, respectively (Fig. 2). Diffraction peaks assigned to brucite and calcite disappeared after 1 day, respectively. The chrysotile diffraction intensity decreased with increasing dissolution time, which means the collapse of the crystal structure of chrysotile. As the dissolution time progressed, halo at 2θ = 15–30°, attributed to amorphous silica, appeared along with weak chrysotile peaks.

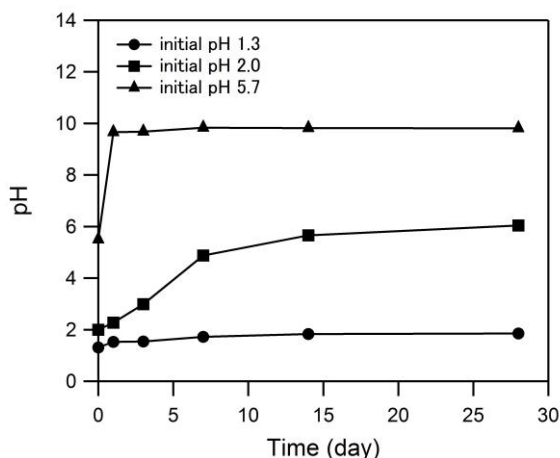


Figure 2. Solution pH values as a function of time.

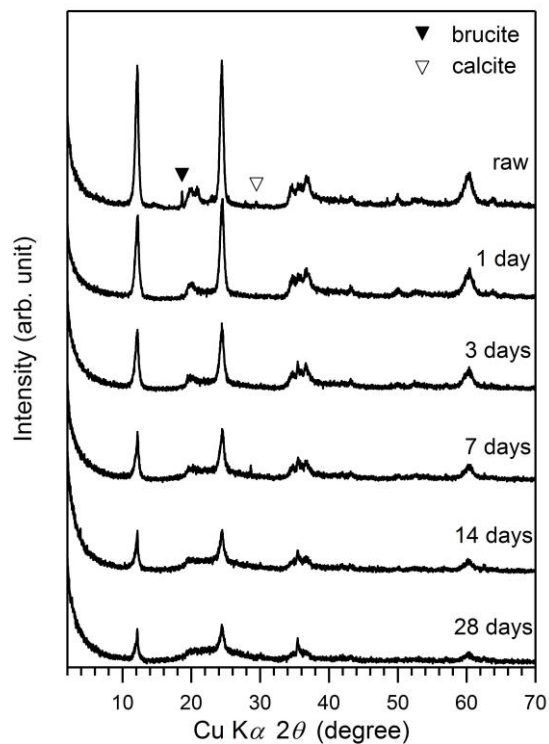


Figure 3. XRD patterns obtained for raw chrysotile and for samples treated with nitric acid solution at pH 1.3 for 1–28 days.

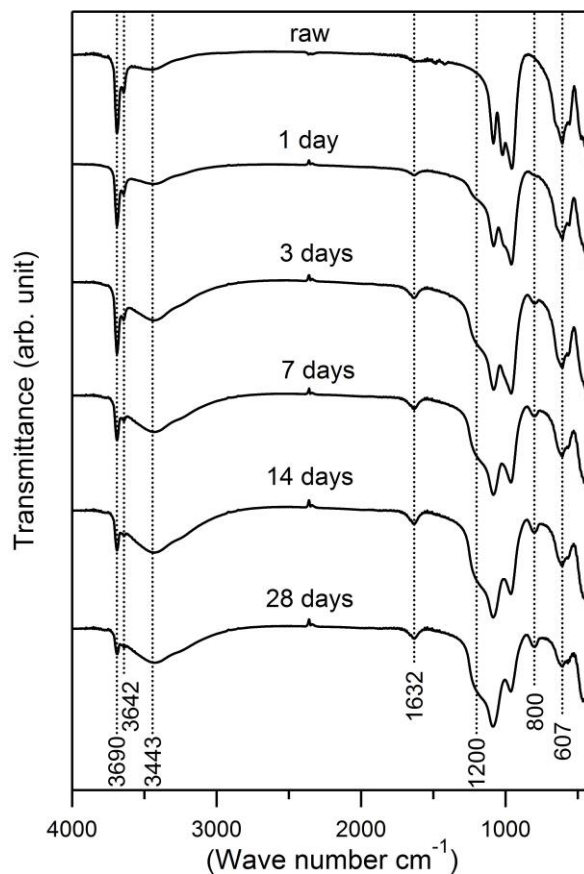


Figure 4. FTIR spectra obtained for raw chrysotile and for samples treated with nitric acid solution at pH 1.3 for 1–28 days.

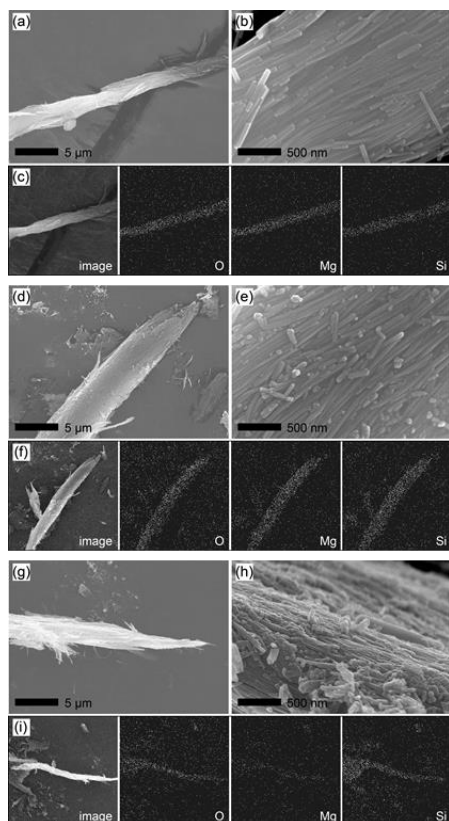


Figure 5. (a, d, g) Standard and (b, e, h) high-magnification FE-SEM images of chrysotile (a, b) raw and (d, e, g, h) treated in nitric acid solution at pH 1.3 for (d, e) 3 days and (g, h) 28 days together with elemental mapping images of (c) raw chrysotile and treated in nitric acid solution at pH 1.3 for (f) 3 days and (i) 28 days.

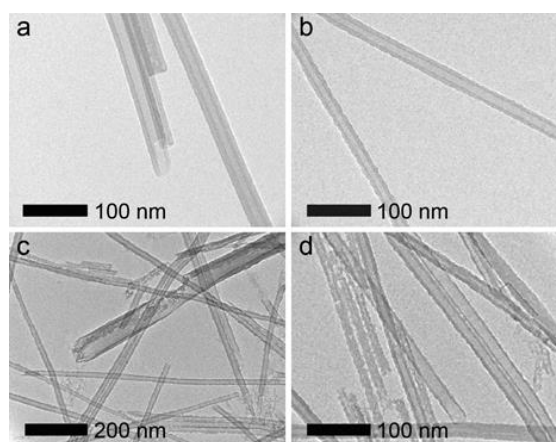


Figure 6. TEM images of chrysotile: (a) raw and (b, c, d) treated in nitric acid solution at pH 1.3 for (b) 3 days and (c, d) 28 days.

The effects of pH on the short-range order in chrysotile are highlighted in the FT-IR spectra recorded for raw chrysotile and for samples treated with nitric acid solution at pH 1.3 for 1–28 days (Fig. 4). The assignments of the different FT-IR bands are based on those reported in previous studies (Van Der Marel *et al.*, 1976; Anbalagan *et al.*, 2010). For raw chrysotile, stretching bands attributed to external and inner Mg-OH groups are observed at 3690 and 3642 cm^{-1} , respectively. The bands at 1084, 1020, and 957 cm^{-1} are attributed to Si-O-Si vibrations in the tetrahedral sheets, while the band at 607 cm^{-1} arises from

inner Mg-OH vibrations and the peak at 434 cm^{-1} is due to Mg-OH translation or Si-O bending. In the spectra of the samples treated with nitric acid solution, the bands at 3443 and 1632 cm^{-1} , assigned to adsorbed water, are more intense than those recorded for raw chrysotile. This phenomenon is due to the higher adsorbed water content on the treated sample, and it has also been reported in previous study (Hongo, 2016). The bands attributed Mg-OH groups at 3690 , 3642 and 607 cm^{-1} shows a pronounced decrease in intensity as the treatment time progressed. The decrease of these bands indicates that the octahedral sheets of magnesium hydroxide in chrysotile are destroyed (Mendelovici *et al.*, 2001). The acid-induced degradation of the octahedral sheets proceeded as dissolution time progressed. The bands assigned to Si-O-Si vibrations between 860 and 1450 cm^{-1} broaden, with broad bands being characteristic of free silica. The bands are accompanied by an appearance and an increase in the intensity of the band at 1200 cm^{-1} assigned to the Si-O vibration in amorphous silica. This phenomenon has also been observed in other clay minerals subjected to acid treatment, such as Montmorillonite, palygorskite and sepiolite (Prakash *et al.*, 1995; Myriam *et al.*, 1998). The additional peak that appears at 800 cm^{-1} is due to the formation of free amorphous silica. From the above results, since Mg preferentially dissolved than Si, the remaining Si component produces amorphous silica.

Under SEM the raw chrysotile displays heterogeneous bundles of chrysotile fibers (Fig. 5a). At greater magnification the alignment of the fibers becomes apparent (Fig. 5b). The fibers in each bundle are several tens of nanometers in diameter and vary in length from approximately 100 nm to well over $1\text{ }\mu\text{m}$. Elemental mapping images of the raw chrysotile show O, Mg and Si were evenly distributed over the bundle (Fig. 5c). The SEM image of the sample treated with nitric acid solution at pH 1.3 for 3 days shows fiber bundles, but short fibers were observed on the surface of the bundles (Fig. 5 d, e). The short one was less than 100 nm . The elemental mapping images show O, Mg and Si were evenly distributed over the bundle (Fig. 5f), though Mg (41%) dissolved more than Si (6%) (Fig. 1). This phenomenon is thought to be due to the dissolution reaction proceeds from the fibers on the surface of the fiber bundle; that is, as the analysis depth for EDX is typically a few micrometers, the data also contains information on mostly undissolved fibers inside the bundle. The SEM image of the sample treated with nitric acid solution at pH 1.3 for 28 days shows more shortened fibers ($\sim 30\text{--}100\text{ nm}$), which were observed on the surface of the bundles (Fig. 5 g, h). The

Figure 5. (a, d, g) Standard and (b, e, h) high-magnification FE-SEM images of chrysotile (a, b) raw and (d, e, g, h) treated in nitric acid solution at pH 1.3 for (d, e) 3 days and (g, h) 28 days together with elemental mapping images of (c) raw chrysotile and treated in nitric acid solution at pH 1.3 for (f) 3 days and (i) 28 days.

elemental mapping images show O and Si were evenly distributed over the bundle, and the Mg was hardly detected (Fig. 5i). This indicates that dissolution proceeds

from the surface towards the interior of the bundles. The dissolution reaction leads the shortening and peeling the fibers on the surface and gradually thinning the bundle. The dissolution process of chrysotile was proposed as a shrinking fiber model, it was confirmed by this study (Hume & Rimstidt, 1992).

TEM images obtained for raw chrysotile and for samples treated with nitric acid solution at pH 1.3 for 3 or 28 days are shown in Fig. 6a-d. In raw chrysotile, the nanotubes have inner and outer diameters of $6\text{--}10$ and $24\text{--}38\text{ nm}$, respectively (Fig. 6a). The sample treated for 3 days have a similar hollow structure but the outer surface, which was smooth before nitric acid treatment, became rough (Fig.

Figure 6. TEM images of chrysotile: (a) raw and (b, c, d) treated in nitric acid solution at pH 1.3 for (b) 3 days and (c, d) 28 days.

6b). This suggests that dissolution reaction initially proceeds the outermost octahedral sheet of magnesium hydroxide. Fibers are also observed in the TEM image of the sample treated for 28 days (Fig. 6c, d). Sheets, which was derived from unrolling the rolled structure, was confirmed, while the fibers in which the hollow structure was maintained were confirmed (Fig. 6c). In addition, Fibers as derived from connected nanoparticles, which were obtained by destroying the hollow structure with separate inner and outer diameters no longer apparent, were observed (Fig. 6d).

4. Conclusions

Chrysotile was dissolved in solutions at pH 1.3, 2.0 or 5.7. Chrysotile becomes more soluble at lower pH values, whereby Mg is dissolved more readily than Si. At pH 1.3, both Mg and Si continued to dissolve for 28 days, and the extent of dissolution after 28 days of Mg was approximately four times greater than that of Si. The release of OH^- groups and Mg^{2+} ions from the octahedral sheets of magnesium hydroxide increases the pH of the solvent after dissolution. XRD and FT-IR data revealed that the chrysotile crystal structure collapsed and amorphous silica was formed as the dissolution time progressed. Following dissolution at pH 1.3 at 3 days, the outer surface of the initially smooth chrysotile fibers became rough, but their hollow structure and the characteristic fiber bundles were retained. After 28 days, samples that were altered into sheet-like form or fiber-like form formed by connecting nanoparticles were confirmed, while there were fibers maintaining hollow structure.

References

Aguado J., Arsuaga J.M., Arencibia A., Lindo M. and Gascón V. (2009), Aqueous heavy metals removal by adsorption on amine-functionalized mesoporous silica, *Journal of Hazardous Materials*, **163**, 213-221.

- Allen S.J., McKay G. and Khader K.Y.H. (1989), Intraparticle diffusion of a basic dye during adsorption onto Sphagnum Peat, *Environmental Pollution*, **56**, 39-50.
- Areco M.M. and Afonso M.S. (2010), Copper, zinc, cadmium and lead biosorption by *Gymnogongrus torulosus*. Thermodynamics and kinetics studies, *Colloids and Surfaces B: Biointerfaces*, **81**, 620-628.
- Axtell N.R., Sternberg S.P.K. and Claussen K. (2003), Lead and nickel removal using *Microspora* and *Lemna minor*, *Bioresource Technology*, **89**, 41-48.
- Bhattacharya A.K., Mandal S.N., and Das S.K. (2006), Adsorption of Zn (II) from aqueous solution by using different adsorbents, *Chemical Engineering Journal*, **123**, 43-51.
- Bulut Y. and Tez Z. (2007), Adsorption studies on ground shells of hazelnut and almond, *Journal of Hazardous Materials*, **149**, 35-41.
- Çalışkan N., Kul A.R., Alkan S., Gogut E.G. and Alacabey I. (2011), Adsorption of zinc (II) on diatomite and manganese-oxide-modified diatomite: A kinetic and equilibrium study, *Journal of Hazardous Materials*, **193**, 27-36.
- Cheremisinoff P.N. (1995), *Handbook of Water and Wastewater Treatment Technology*, Marcel Dekker Inc., New York.
- Anbalagan G., Sivakumar G., Prabakaran S. and Gunasekaran S. (2010) Spectroscopic characterization of natural chrysotile, *Vibrational Spectroscopy*, **52**, 122–127.
- Brindley G.W. and Brown G. (1980) *Crystal Structure of Clay Minerals and Their X-ray Identification*, Mineralogical Society, London.
- Dana J.D., Hurlbut C.S. and Klein D. (1977) *Manual of Mineralogy*, John Wiley & Sons, New York.
- Długogorski B.Z. and Balucan R.D. (2014) Dehydroxylation of serpentine minerals: Implications for mineral carbonation, *Renewable & Sustainable Energy Reviews*, **31**, 353–367.
- Foresti E., Gazzano M., Gualtieri A.F., Lesci I.G., Lunelli B., Pecchini G., Renna E. and Roveri N. (2003) Determination of low levels of free fibres of chrysotile in contaminated solids by X-ray diffraction and FT-IR spectroscopy, *Analytical and Bioanalytical Chemistry*, **376**, 653–658.
- Hongo T. (2016), Dissolution of the chrysotile structure in nitric-acid solutions at different pH, *Clay Minerals*, **51**, 715-722.
- Hume L.A. and Rimstidt J.D. (1992) The biodurability of chrysotile asbestos, *American Mineralogist*, **77**, 1129–1128.
- Kumar P., Jasra R.V. and Bhat T.S.G. (1995) Evolution of Porosity and Surface Acidity in Montmorillonite Clay on Acid Activation, *Industrial & Engineering Chemistry Research*, **34**, 1440-1448.
- Liu K., Feng Q., Yang Y. Zhang G., Ou L. and Lu Y. (2007) Preparation and characterization of amorphous silica nanowires from natural chrysotile, *Journal of Non-crystalline Solids*, **353**, 1534–1539.
- Mendelovici E., Frost R.L. and Klopogge J.T. (2001) Modification of Chrysotile Surface by Organosilanes: An IR-Photoacoustic Spectroscopy Study, *Journal Colloid and Interface Science*, **238**, 273–278.
- Mossman B.T., Bignon J., Corn M., Seaton A. and Gee J.B.L. (1990) Asbestos: Scientific developments and implications for public policy, *Science*, **247**, 294-301.
- Myriam M., Suárez M. and Martín-Pozas J.M. (1998) Structural and Textural Modifications of Palygorskite and Sepiolite under Acid Treatment, *Clays and Clay Minerals*, **46**, 225-231.
- Pundsack F.L. (1955) The properties of Asbestos. I. The colloidal and surface chemistry of chrysotile, *The Journal of Physical Chemistry*, **59**, 892–895.
- Van Der Marel H.W. and Beutelspacher H. (1976) *Atlas of Infrared Spectroscopy of Clay Minerals and Their Admixtures*. Elsevier Science, Amsterdam.